

Supporting Information

Experimental evaluation of indium (I) iodide as lead-free perovskite-inspired material for photovoltaic applications

Marina I. Ustinova,^{a*} Sergey D. Babenko,^b Sergey Yu. Luchkin,^c Filipp S. Talalaev,^a Denis V. Anokhin,^{a,d} Selina Olthof,^e and Pavel A. Troshin^a

^a Institute for Problems of Chemical Physics RAS (IPCP RAS), Academician Semenov St. 1, Chernogolovka, 142432, Russia

^b Chernogolovka branch of the N.N. Semenov Federal Research Center for Chemical Physics RAS, Academician Semenov St.1/10 Chernogolovka 142432, Russia

^c Skolkovo Institute of Science and Technology, Nobel St. 3, Moscow, 121205, Russia

^d Lomonosov Moscow State University, 1 Leninskie Gory, Moscow, 119991, Russia

^e Department Chemie, Universität zu Köln, Greinstrasse 4-6, Köln, 50939, Germany

Corresponding Author

Marina I. Ustinova * E-mail: ustinova1712@gmail.com

Content

Experimental Section	2
Materials.....	2
Fabrication of devices with vertical geometry	2
Fabrication of lateral InI devices.....	3
Characterization of InI devices	3
Characterization of InI films	3
Table S1. The characteristics of solar cells (ITO/SnO ₂ /PCBM/InI/PTA/MoO ₃ /Ag) with the InI film thickness of 200 nm.	5
Figure S1. The UPS and IPES spectra for a series of samples: ITO/SnO ₂ , ITO/SnO ₂ /PCBM, ITO/SnO ₂ /PCBM/InI, and ITO/SnO ₂ /PCBM/InI/PTA.	6
Figure S2. Characteristics of InI-based photodetector devices with lateral and vertical geometry measured under different illumination intensities and plotted as a function of bias voltage: photodetectivity $P=(I_{\text{light}}-I_{\text{dark}})/I_{\text{dark}}$ (a, b); responsivity $R=(I_{\text{light}}-I_{\text{dark}})/W$ (c, d); specific detectivity $D = R/(2eJ_{\text{dark}})^{1/2}$ (e, f).	7
Figure S3. The magnitude of the device's photoresponse as a function of the bias voltage for vertical (a) and lateral (b) InI-based photodetectors measured using 466 nm LED illumination with 80 mW·ms ⁻¹ incident power. The calculated resistances of photodetectors (R_{ph}) are 0.15 and 0.14 GOhm, respectively.	8
Figure S4. The device response to the sequence of the light pulses (466 and 405 nm for vertical and lateral geometries, respectively) modulated with the following frequencies: 133 Hz for vertical (a) and 1 Hz for lateral (b) architectures.	8

Figure S5. The electric circuit with a simplified photodetector equivalent scheme used to estimate the effective charge carrier lifetimes (t_0) ($R_{ph} = 0.15$ and 0.14 GOhm for vertical and lateral InI devices, respectively), R_{Load} was varied from 0.2215 to 1000 kOhm.	9
Figure S6. The dependence of the photoresponse of devices assembled in the vertical (a) and lateral (b) geometries on the load resistances (1 ms 466 nm LED pulse was used for excitation). The linear dependences of $1/\tau$ on $1/R_{Load}$ used to estimate the effective charge carrier lifetimes in InI photodetectors (τ_0) and the photodetector capacity (C).	10
Table S2. The calculated $R_{Load}C$ time constants and the cut-off frequency (f) of the InI photodetectors at different load resistances (R_{Load}).	11
Table S3. The performance and structural orientation of Bi(III) halides in devices based on the previous reports.....	12

Experimental Section

Materials

The following anhydrous reagents and solvents were purchased from Sigma-Aldrich: InI (99.999% purity grade), ZnS (99.99%), MoO₃ (99.5%). [6,6]-phenyl-C₆₁-butyric acid methyl ester (PCBM, 99.9%) was purchased from FOMaterials Ltd. (Russia). ITO glass (15 Ohm/sq.) was purchased from Kintec, China. Colloidal dispersion aqueous SnO₂ (15%) was obtained from Alfa-Aesar. (Poly[bis(4-phenyl)(4-methylphenyl)amine] (PTA) was synthesized according to the known procedure.¹⁻²

Fabrication of devices with vertical geometry

SnO₂ precursor solution was prepared by dilution of commercial 15% aqueous SnO₂ colloidal dispersion with deionized water to obtain 10% final concentration; an aliquot of this solution (40 μ l) was spin-coated on ITO glass at 5000 rpm for 40 sec. The obtained films were initially annealed at 175 °C for 15 min on a hot plate in the air and then in a nitrogen glove box at 150 °C for an additional 10 min. The SnO₂ films were passivated by spin-coating 15 mg ml⁻¹ PCBM solution in toluene (3000 rpm, 30 sec) followed by thermal annealing of the obtained films at 100 °C for 10 min. The absorber indium iodide (InI) layer with a thickness of 200 or 600 nm was deposited on the top of the PCBM passivation layer by thermal evaporation *in vacuo* (10⁻⁵ mbar) from a quartz crucible at 200-230°C at 1 Å/s rate. Afterward, the absorber films were annealed at 150 °C for 5 min. The PTA hole-transport layer was deposited by spin-coating a solution of this material in toluene (concentration 2.5 mg ml⁻¹) at 1000 rpm. The top contact composed of 15 nm MoO_x (electron-blocking layer) and 100 nm Ag was deposited by thermal evaporation of MoO₃

and metallic silver *in vacuo* (10^{-5} mbar). The obtained devices were additionally annealed in an inert nitrogen atmosphere at 100 °C for 5 min to improve PCE.

Fabrication of lateral InI devices

InI films with a thickness of 100 nm were deposited on the borosilicate glass substrates with the area of 1.25×1.25 cm² using thermal evaporation *in vacuo* (10^{-5} bar) from a quartz crucible at 200-230°C at 1 Å/s rate. Afterward, the films were annealed at 175 °C for 5 min. Gold electrodes (100 nm) were evaporated (10^{-5} bar) on top of InI films via a shadow mask defining the channel length and width as 50 μm and 2 mm, respectively.

Characterization of InI devices

Electrical characteristics of the InI-based devices were measured using Keithley 2612A dual-channel and Advantest 6240A single-channel source-measurement units. The J-V characteristics of the InI solar cells were measured in an inert nitrogen atmosphere inside the glove box using the simulated AM1.5G illumination ($100 \text{ mW} \cdot \text{cm}^{-2}$) and provided by Newport Verasol AAA class solar simulator. The intensity of the illumination was checked before each measurement using a calibrated silicon diode with a known spectral response. The EQE spectra were measured using a PV Instruments system integrated into MBraun glove box. The xenon short-arc lamp (150 W, USHIO Inc., Japan) was used as a light source for EQE measurements, while the bias light ($100 \text{ mW} \cdot \text{cm}^{-2}$) was provided by OSRAM halogen lamp (75 W) and the beam focusing optical system.

The transient responses were recorded using a G5-63 signal generator, driving a LED illumination with a peak wavelength at 466 nm with $80 \text{ mW} \cdot \text{ms}^{-1}$ power and a 532 nm laser (DTL-31QT).

The device photoresponse was measured using a series of R_{Load} resistors connected in the circuit as shown in Fig. S5 with an 8-bit digital oscilloscope PCS500 (Velleman Instruments, Taiwan).

Characterization of InI films

UV-vis absorbance spectra were recorded in an inert atmosphere using AvaSpec-2048-2 fiber spectrometer integrated with MBraun glove box. XRD patterns were collected using a Bruker D8 diffractometer with CuK_α source. GIWAXS measurements were performed in European Synchrotron Radiation Facility (Grenoble, France) on BM26 beamline. AFM images were obtained using a Cypher ES microscope (Asylum Research, Oxford Instruments) installed in an Ar-filled glovebox. UPS and IPES spectra for the series of samples ITO/SnO₂, ITO/SnO₂/PCBM, ITO/SnO₂/PCBM/InI, and ITO/SnO₂/PCBM/InI/PTA were measured as

described previously.³ The samples were transferred into the ultra high vacuum system under nitrogen atmosphere and were therefore not exposed to air.

Table S1. The characteristics of solar cells (ITO/SnO₂/PCBM/InI/PTA/MoO₃/Ag) with the InI film thickness of 200 nm.

Passivation layer	V_{oc}, mV	J_{sc}, mA cm⁻²	FF, %	PCE, %
PCBM	496	2.83	54	0.65
Reference sample without passivation layer	279	2.21	34	0.2

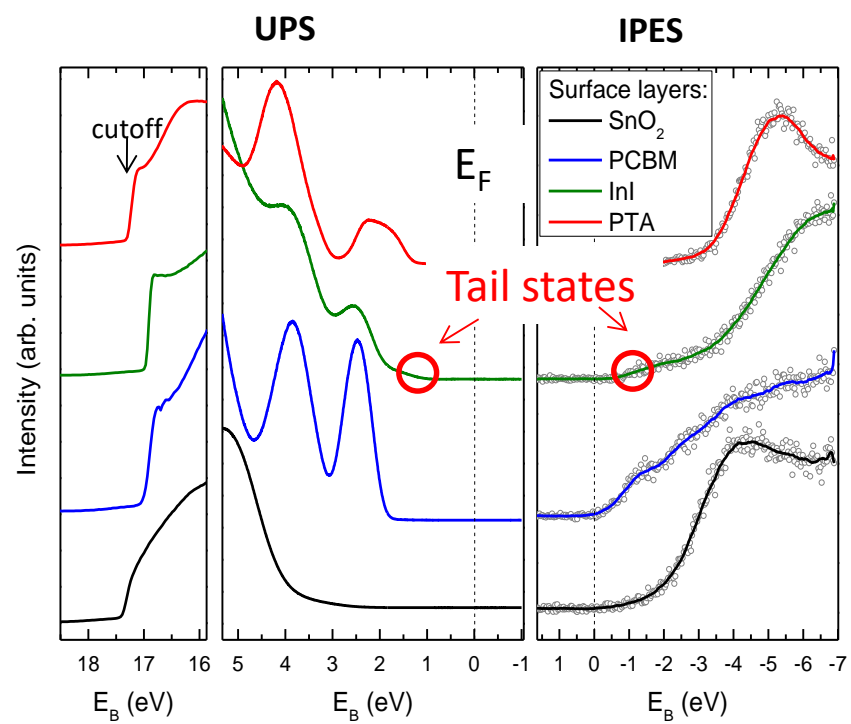


Figure S1. The UPS and IPES spectra for a series of samples: ITO/SnO₂, ITO/SnO₂/PCBM, ITO/SnO₂/PCBM/InI, and ITO/SnO₂/PCBM/InI/PTA.

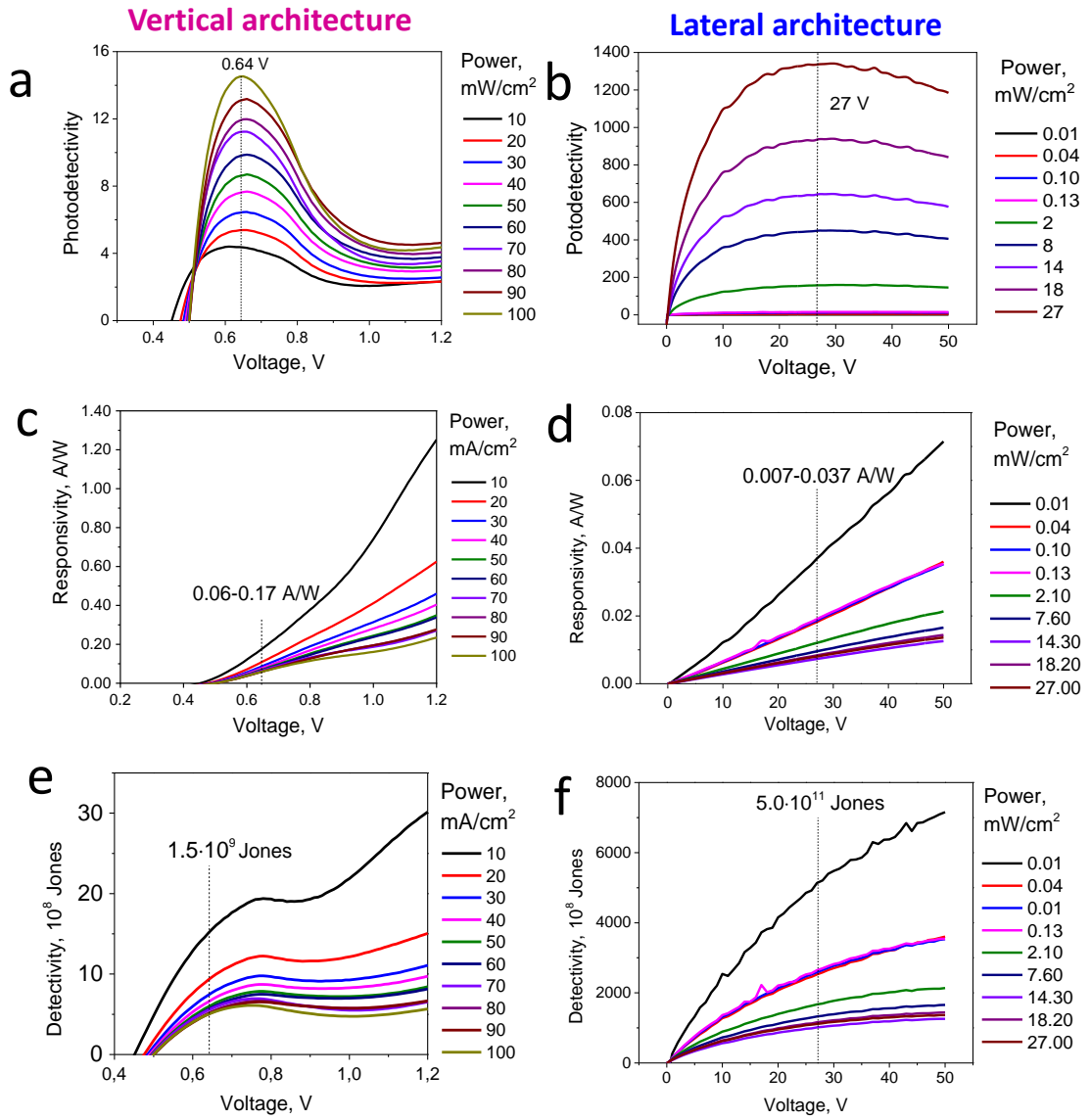


Figure S2. Characteristics of InI-based photodetector devices with lateral and vertical geometry measured under different illumination intensities and plotted as a function of bias voltage: photodetectivity $P=(I_{\text{light}}-I_{\text{dark}})/I_{\text{dark}}$ (a, b); responsivity $R=(I_{\text{light}}-I_{\text{dark}})/W$ (c, d); specific detectivity $D = R/(2eJ_{\text{dark}})^{1/2}$ (e, f).

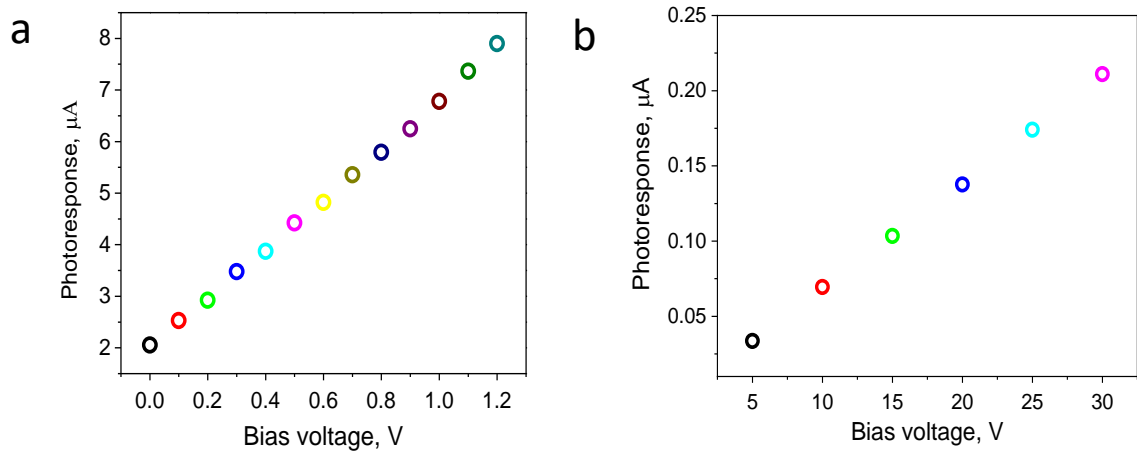


Figure S3. The magnitude of the device's photoresponse as a function of the bias voltage for vertical (a) and lateral (b) InI-based photodetectors measured using 466 nm LED illumination with $80 \text{ mW} \cdot \text{ms}^{-1}$ incident power. The calculated resistances of photodetectors (R_{ph}) are 0.15 and 0.14 GOhm, respectively.

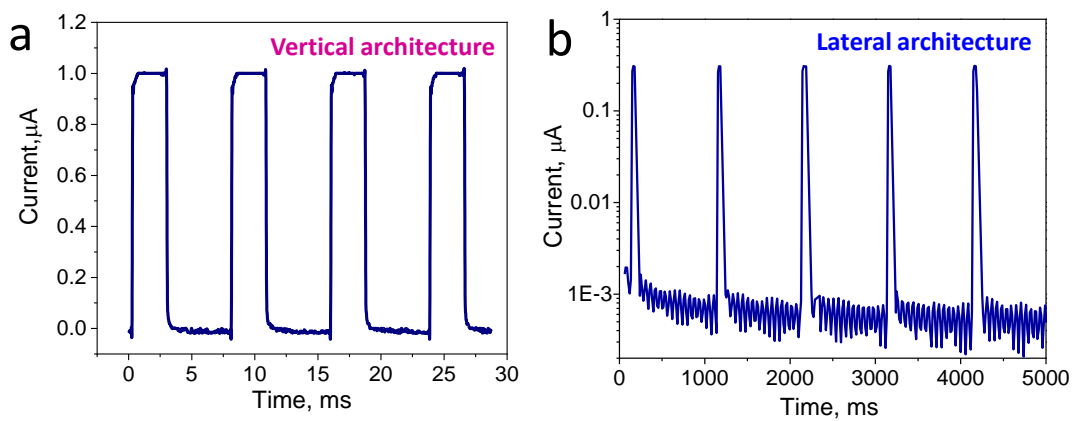
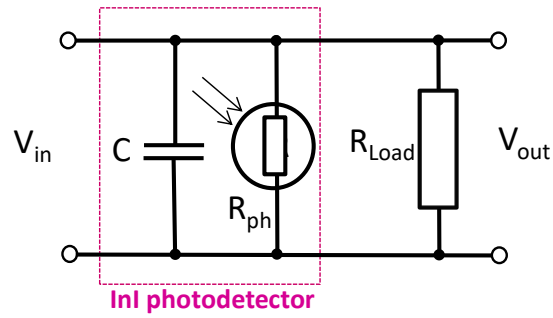


Figure S4. The device response to the sequence of the light pulses (466 and 405 nm for vertical and lateral geometries, respectively) modulated with the following frequencies: 133 Hz for vertical (a) and 1 Hz for lateral (b) architectures.



$$\frac{1}{t} = \frac{1}{t_0} + \frac{1}{R_{Load} \cdot C}$$

t - charge carrier lifetime

Figure S5. The electric circuit with a simplified photodetector equivalent scheme used to estimate the effective charge carrier lifetimes (t_0) ($R_{ph} = 0.15$ and 0.14 GOhm for vertical and lateral InI devices, respectively), R_{Load} was varied from 0.2215 to 1000 kOhm.

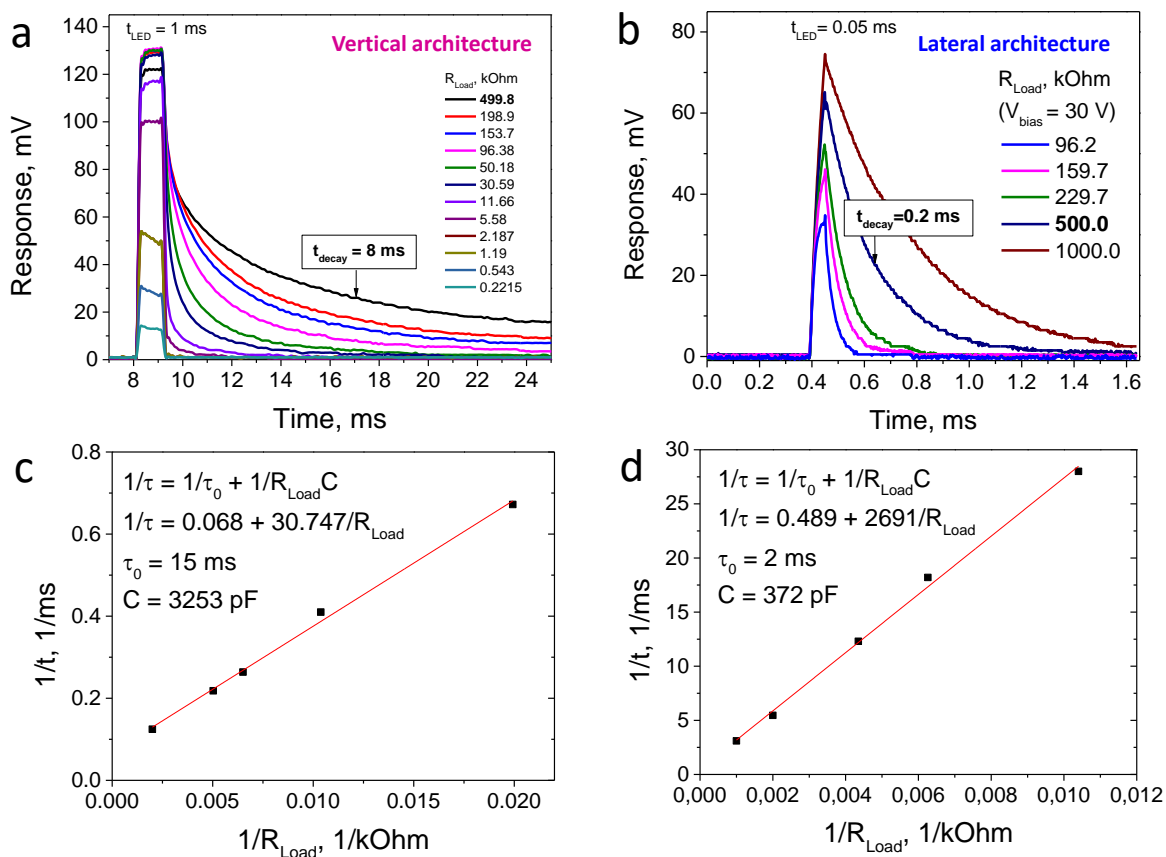


Figure S6. The dependence of the photoresponse of devices assembled in the vertical (a) and lateral (b) geometries on the load resistances (1 ms 466 nm LED pulse was used for excitation). The linear dependences of $1/\tau$ on $1/R_{Load}$ used to estimate the effective charge carrier lifetimes in InI photodetectors (τ_0) and the photodetector capacity (C).

Table S2. The calculated $R_{Load}C$ time constants and the cut-off frequency (f) of the InI photodetectors at different load resistances (R_{Load}).

R_{Load} , kOhm	$R_{Load}C$ time constant, ms	Cut-off frequency (f), kHz $f = \frac{1}{3R_{Load}C}$
Vertical InI devices		
499.8	1.6258	0.2
198.9	0.6470	0.5
153.7	0.5000	0.7
96.38	0.3135	1.1
50.18	0.1632	2.0
30.59	0.0995	3.3
11.66	0.0379	8.8
5.58	0.0182	18.4
2.187	0.0071	46.9
1.19	0.0039	86.1
0.543	0.0018	188.7
0.2215	0.0007	462.6
Lateral InI devices		
1000	0.0370	9.0
500	0.0185	18.0
229.7	0.0085	39.2
159.7	0.0059	56.4
96.2	0.0036	93.6

Table S3. The performance and structural orientation of Bi(III) halides in devices based on the previous reports.

Vertical device geometry					Orientation with respect to the substrate
Device architecture	PCE, %	V_{oc} , mV	J_{sc} , $\text{mA}\cdot\text{cm}^{-2}$	FF, %	
ITO/TiO ₂ /(N-MePy){[Bi ₃ I ₁₀]}/P3HT/Au ⁴	0.2	140	0.49	32	parallel
ITO/TiO ₂ /(N-EtPy){[Bi ₃ I ₁₀]}/P3HT/Au ⁴	0.12	572	0.36	58	parallel
ITO/TiO ₂ /(N-methylquinolinium){[BiI ₄]}/P3HT/Au ⁴	0.08	620	0.48	26	vertical and parallel
ITO/SnO ₂ /PC ₆₁ BM/InI/PTA/MoO ₃ /Ag (<i>this work</i>)	1.0	540	3.8	51	parallel
Lateral device geometry					
	Photodetectivity		Responsivity, $\text{A}\cdot\text{W}^{-1}$		
glass/(N-EtPy){[Bi ₃ I ₁₀]}+I ₂ /Au ⁴	>10 (405 nm, 70 mW cm^{-2} , $V_{bias}=100\text{V}$)		unknown		parallel
SiO ₂ /octadecyltrichlorosilane/graphene/BiI ₃ ⁵	~18 (0.2 mW cm^{-2} , $V_{drain}=0.5\text{V}$, $V_{gate}=0\text{V}$)		$6\cdot 10^6$		parallel
Glass/InI/Au (<i>this work</i>)	$1.4\cdot 10^3$		0.05		parallel

References

1. Tsarev, S.; Yakushchenko, I. K.; Luchkin, S. Y.; Kuznetsov, P. M.; Timerbulatov, R. S.; Dremova, N. N.; Frolova, L. A.; Stevenson, K. J.; Troshin, P. A., A New Polytriarylamine Derivative for Dopant-Free High-Efficiency Perovskite Solar Cells. *Sustain. Energy Fuels* **2019**, *3*(10), 2627-2632.
2. Yakushchenko, I. K.; Kaplunov, M. G.; Efimov, O. N.; Belov, M. Y.; Shamaev, S. N., Polytriphenylamine Derivatives as Materials for Hole Transporting Layers in Electroluminescent Devices. *Phys. Chem. Chem. Phys.* **1999**, *1*(8), 1783-1785.
3. Tao, S.; Schmidt, I.; Brocks, G.; Jiang, J.; Tranca, I.; Meerholz, K.; Olthof, S., Absolute energy level positions in tin-and lead-based halide perovskites. *Nature communications* **2019**, *10*(1), 1-10.
4. A. N. Usoltsev, M. Elshobaki, S. A. Adonin, L. A. Frolova, T. Derzhavskaya, P. A. Abramov, D. V. Anokhin, I. V. Korolkov, S. Y. Luchkin, N. N. Dremova, K. J. Stevenson, M. N. Sokolov, V. P. Fedin and P. A. Troshin, *J. Mater. Chem. A*, 2019, **7**, 5957–5966.
5. P. H. Chang, C. S. Li, F. Y. Fu, K. Y. Huang, A. S. Chou and C. I. Wu, *Adv. Funct. Mater.*, 2018, **28**, 1870160.